Title

Drug–drug conjugates of MEK and Akt inhibitors for RAS-mutant cancers

Authors

Hikaru Fujita[a,*], Sachiko Arai[b], Hiroshi Arakawa[a], Kana Hamamoto[a], Toshiyuki Kato[a], Tsubasa Arai[a], Nanaka Nitta[a], Kazuki Hotta[a], Natsuko Hosokawa[c], Takako Ohbayashi[c], Chiaki Takahashi[b], Yasuhide Inokuma[d,e], Ikumi Tamai[a], Seiji Yano[b], Munetaka Kunishima[a,f,*], Yoshihiro Watanabe[g,*]

Affiliations

[a] Faculty of Pharmaceutical Sciences, Institute of Medical, Pharmaceutical, and Health Sciences, Kanazawa University, Kakuma-machi, Kanazawa, Ishikawa 920-1192, Japan.

[b] Division of Medical Oncology, Cancer Research Institute, Kanazawa University, 13-1 Takara-machi, Kanazawa, Ishikawa 920-0934, Japan.

[c] Department of Rheumatology, Kanazawa University Hospital, 13-1 Takara-machi, Kanazawa, Ishikawa 920-0934, Japan.

[d] Division of Applied Chemistry, Faculty of Engineering, Hokkaido University, Kita 13, Nishi 8, Kita-ku, Sapporo, Hokkaido, 060-8628 Japan.

[e] Institute for Chemical Reaction Design and Discovery (WPI-ICReDD), Hokkaido University, Kita 21, Nishi 10, Kita-ku, Sapporo, Hokkaido, 001-0021 Japan.

[f] Faculty of Pharmaceutical Sciences, Kobe Gakuin University, 1-1-3 Minatojima, Chuo-ku, Kobe, Hyogo 650-8586, Japan.

[g] Innovative Clinical Research Center, Kanazawa University Hospital, 13-1 Takara-machi, Kanazawa, Ishikawa 920-0934, Japan.

Corresponding authors

E-mail addresses:

hfujita@staff.kanazawa-u.ac.jp (H. Fujita)

kunisima@pharm.kobegakuin.ac.jp (M. Kunishima)

yoshi.watanabe@staff.kanazawa-u.ac.jp (Y. Watanabe)

Keywords

RAS-mutations, downstream signal, drug–drug conjugate (DDC), trametinib, Akt inhibitor, linker

Abbreviations

DDC, drug–drug conjugate; DMSO, dimethyl sulfoxide; DMT-MM, 4-(4,6-dimethoxy-1,3,5-triazin-2-yl)-4-methylmorpholinium chloride; ERK, extracellular signal-regulated kinase; KSR, Kinase suppressor of Ras; LG, leaving group; MEK, MAPK/ERK kinase; mTOR, mammalian target of rapamycin; NADPH, nicotinamide adenine dinucleotide phosphate hydrogen; NMM, *N*-methylmorpholine; PARP, poly (ADP-

ribose) polymerase; PD, pharmacodynamics; PI3K, phosphoinositide 3 kinase; PK, pharmacokinetics; Raf, rapidly accelerated fibrosarcoma; RAS, rat sarcoma; TFA, trifluoroacetic acid.

Graphical abstract

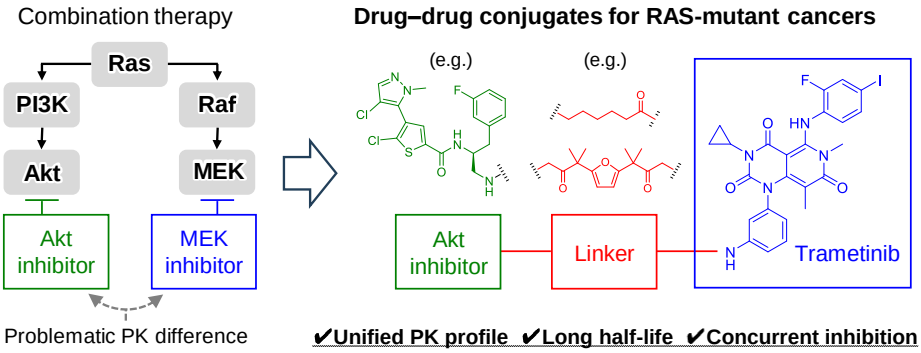

Abstract

Controlling RAS mutant cancer progression remains a significant challenge in developing anticancer drugs. Whereas Ras G12C-covalent binders have received clinical approval, the emergence of further mutations, along with the activation of Ras-related proteins and signals, has led to resistance to Ras binders. To discover novel compounds to overcome this bottleneck, we focused on the concurrent and sustained blocking of two major signaling pathways downstream of Ras. To this end, we synthesized 25 drug–drug conjugates (DDCs) by combining the MEK inhibitor trametinib with Akt inhibitors using seven types of linkers with structural diversity. The DDCs were evaluated for their cell permeability/accumulation and ability to inhibit proliferation in RAS-mutant cell lines. A representative DDC was further evaluated for its effects on signaling proteins, induction of apoptosis-related proteins, and the stability of hepatic metabolic enzymes. These *in vitro* studies identified a series of DDCs, especially those containing a furan-based linker, with promising properties as agents for treating RAS-mutant cancers. Additionally, *in vivo* experiments in mice using the two selected DDCs revealed prolonged half-lives and anticancer efficacies comparable to those of trametinib. The PK profiles of trametinib and the Akt inhibitor were unified throug the DDC formation. The DDCs developed in this study have potential as drug candidates for the broad inhibition of RAS-mutant cancers.

1. Introduction

Mutations in RAS play an important role in tumorigenesis by activating downstream signaling pathways. The spectra of RAS mutations are diverse. For example, multiple mutations such as G12C/D/R/V/W have been observed within the G12 subset in KRAS.[1,2] Whereas approved G12C covalent inhibitors such as sotorasib (AMG510) have shown efficacy in suppressing G12C-mutant cancer progression, other mutations at sites such as G13D, Q61H, and H95D/Q/R have been identified as conferring resistance to the G12C covalent inhibitors.[3–5] In addition, a non-covalent inhibitor, MRTX1133, has been applied to tumors harboring G12D-mutant KRAS.[6] While these advances are significant, they underscore the need for strategically different approaches to KRAS-mutant cancers to address the complexities presented by various mutations.

Clinical trials investigating combination therapies with multiple inhibitors targeting proteins both upstream and downstream of the Ras pathway have shown promise as a therapeutic strategy for RAS-mutant cancers in pancreatic, lung, colon, and other malignancies.[7–10] The cumulative results of both *in vitro* and *in vivo* antiproliferative assays have demonstrated noteworthy potency when used with appropriate drug combinations, suggesting their potential clinical utility. However, discernible tumor regression effects are yet to be observed in patients with RAS-mutant cancers.[11,12] Several plausible explanations have been proposed and require further exploration.[13,14] One possibility is the emergence of resistance due to additional mutations in signaling proteins that are targeted directly or indirectly by co-administered pharmaceutical agents. Another possible factor is the increased expression and activation of Ras and related proteins, which result from decreased feedback mechanisms caused by downstream signaling pathway inhibition. Furthermore, disparities in the PK and PD profiles of individual drugs can increase drug toxicity when used

in combination, which is a significant obstacle in maintaining an adequate safety margin. Developing combination therapies is complex. Even a successful combination of the MEK inhibitor trametinib and the B-Raf inhibitor dabrafenib has different dosing regimens, with dabrafenib administered twice daily and trametinib once daily.[15] The complexity of combination therapies is further exemplified by a phase 1 study combining trametinib with the Akt inhibitor afuresertib in melanoma patients.[11] Notably, dose-limiting toxicity was associated with a high area under the curve of afuresertib, rather than trametinib. With these tolerable dosing regimens, the addition of afuresertib to trametinib did not provide any additional discernible benefits in these patients.

To efficiently eradicate cancers, the selection force of anticancer agents should be maintained at a sufficient level to inhibit the targeted signaling pathways.[16,17] Therefore, new anticancer agents with extended half-lives and stable *in vivo* PK profiles are highly desirable. In this context, drug–drug conjugates (DDCs) have received increasing attention in recent years as dual-targeting inhibitors to overcome the problems of combination therapies.[18–21] For example, one study investigated the *in vivo* anticancer effect of DDCs prepared by covalently attaching an MEK inhibitor (avutometinib) and a PI3K inhibitor (ZSTK474) to a polyethylene glycol linker.[22] However, their cell permeability and *in vivo* PK profiles have not been thoroughly characterized.

Herein, we report novel DDCs comprising a clinically established MEK inhibitor, trametinib, an Akt inhibitor, and structurally diverse linkers. The rationale behind the design of these DDCs stems from the enhanced downstream signaling observed in RAS-mutant cancer cells, which warrants the concurrent inhibition of two key signaling pathways, Raf–MEK–ERK and PI3K–Akt–mTOR.[23–25] The linchpin of these DDCs is trametinib, chosen due to its unique binding properties: its strong affinity (IC_{50} = 0.92–3.4 nM)[26] and extremely slow dissociation ($k_{off} = 1.2 \times 10^{-4}$ sec^{-1})[27] for MEK results in the formation of a highly stable MEK–trametinib complex. This complex dissociates from the Ras/Raf/MEK scaffold into the cytosol.[13,28] Consequently, we anticipate that trametinib-containing DDCs will exhibit prolonged retention within cancer cells, resulting in sustained Akt activity blockade through the Akt inhibitor moiety of the DDCs. Our results suggest that the DDCs developed in this study effectively maintained the properties of trametinib, as demonstrated by *in vitro* and *in vivo* analyses.

2. Results and discussion

2.1. Synthesis and in vitro characterization of the first-series DDCs

2.1.1. Design and synthesis

We planned to extend the linker from the acetamide moiety of trametinib for conjugation to an Akt inhibitor based on the results of a reported study.[27] This study demonstrated that structural modifications to the acetamide moiety did not affect the retained MEK binding of trametinib-based affinity probes in both intracellular and cell-free systems. *N*-Deacetylated trametinib (**1**, Fig. 1A), which bears an aromatic amino group on the trametinib moiety (Tra), was selected as the starting material for DDC synthesis. The linker moiety can be attached to **1** via amidation with a hetero-functionalized linker building block possessing a carboxy group at one end (Fig. 1B). Subsequently, the leaving group (LG) located at the opposite end can

undergo an S_N2-type *N*-alkylation with the amino group of the Akt inhibitor, resulting in DDC formation. The linker length of the DDCs was defined as the number of atoms present in the shortest path connecting the two nitrogen atoms used in the linkage of **1** and the Akt inhibitor.

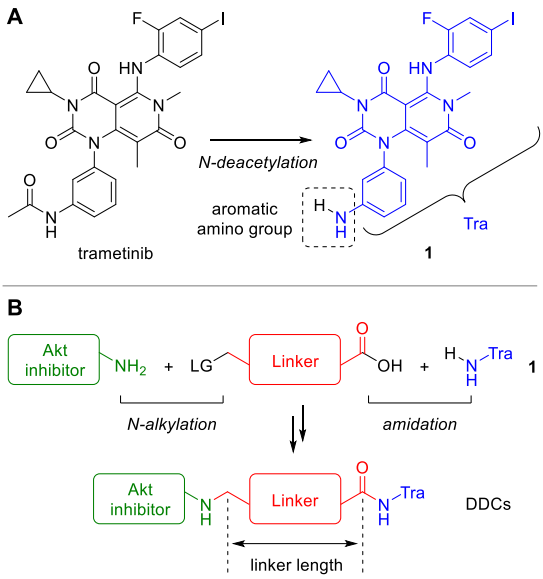

Fig. 1. Molecular design and synthetic strategy of Akt inhibitor–trametinib conjugates. (A) *N*-Deacetylation of trametinib to expose an aromatic amino group as the linker connection site. (B) Conjugation of trametinib and an Akt inhibitor between a hetero-functionalized linker via amidation and subsequent *N*-alkylation.

To systematically evaluate the effect of linker length on the activity, we synthesized DDCs containing aliphatic linkers (L1) of various lengths (Scheme 1). Afuresertib (**A1-NH$_2$**, K_i = 0.08 nM and 2 nM for Akt1 and Akt2, respectively)[8] and MK2206 (**A2-NH$_2$**, IC_{50} = 8 nM and 12 nM for Akt1 and Akt2, respectively)[29] were selected as the Akt inhibitor moiety. In the synthetic schemes, the chemical structures corresponding to the trametinib and Akt inhibitor moieties are represented by "Tra" and "An" (n = 1–4) in blue and green, respectively. The linker moiety is indicated in red. Treatment of trametinib with HCl/EtOH afforded the *N*-deacetylated product **1** in 86% yield. This product was subsequently reacted with bromoacetyl bromide or bromoalkyl-carboxylic acids using DMT-MM[30,31] and *N*-methylmorpholine (NMM), forming bromoalkyl-Tra intermediates **2**–**5** with linker lengths of 2–16 in 72–90% yield. After the alkylative coupling of **2**–**5** with **A1-NH$_2$** or **A2-NH$_2$** in the presence of ^{i}Pr$_2$EtN and NaI, six DDCs (**A1-L1^2-Tra**, **A2-L1^2-Tra**, **A1-L1^6-Tra**, **A2-L1^6-Tra**, **A1-L1^{10}-Tra**, and **A1-L1^{16}-Tra**; the linker length is indicated by the superscript suffix) were obtained in 16–62% yield. Additionally, compound **7**, which bears the linker L1 with a length of 6 but lacks the Akt inhibitor moiety, was synthesized.

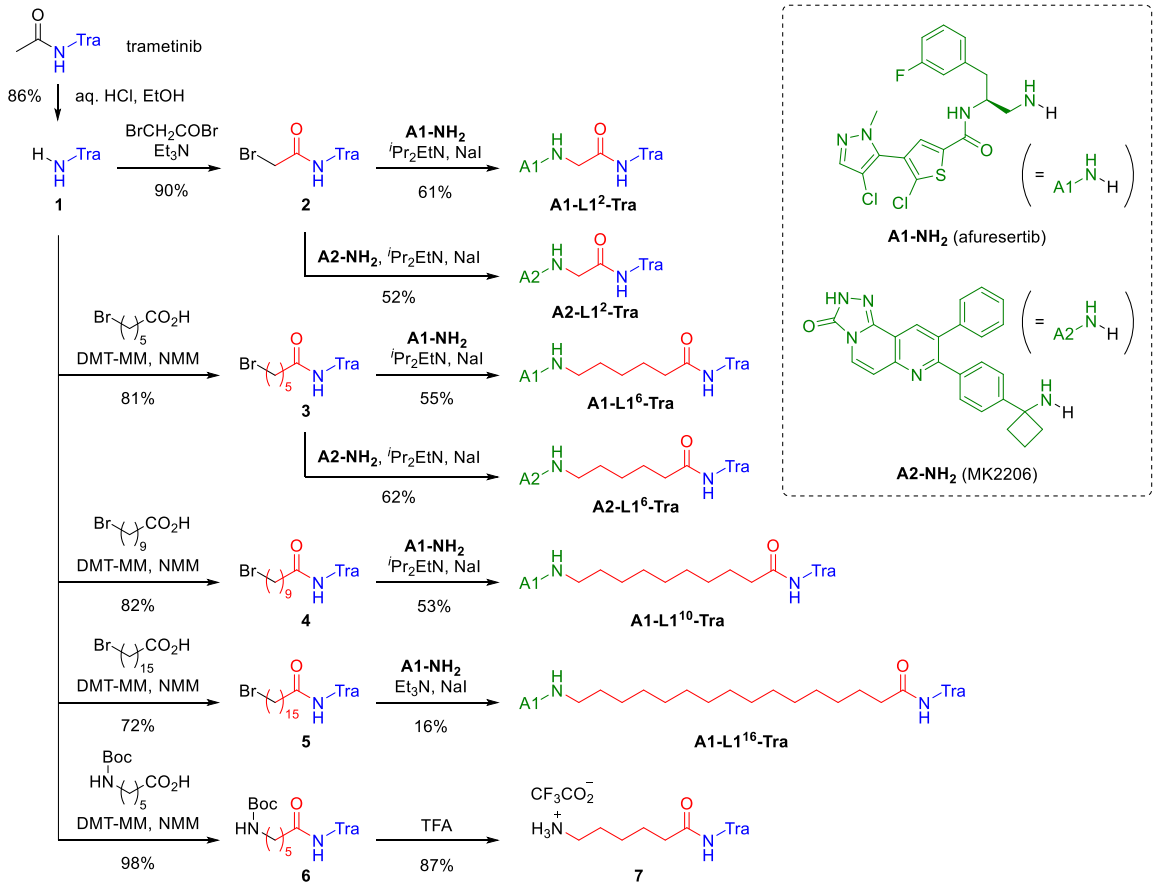

Scheme 1. Synthesis of six DDCs composed of an Akt inhibitor moiety (A1 or A2), linker L1 with a length of 2–16, and Tra.

The use of linker L1 with a length longer than 16 was expected to be unsuitable due to the limited water-solubility of the resulting DCC. To counteract this, we devised oxyethylene-amide linkers (L2) to improve the water solubility (Scheme 2). The synthesis was initiated by the reaction of mono-Boc-protected diamine **8** with diglycolic anhydride, affording carboxylic acid **9**. Sequential conversion, including DMT-MM-mediated amidation with **1**, Boc deprotection, and *N*-acylation with bromoacetyl bromide, afforded bromoalkyl-Tra intermediate **12** (57% yield in three steps). The alkylative coupling of **12** with **A1-NH$_2$** and **A2-NH$_2$** afforded **A1-L2^{22}-Tra** and **A2-L2^{22}-Tra** in 72% and 59% yield, respectively. These DDCs contained the linker L2 with a length of 22. To compare the effect of the conjugation mode of the Akt inhibitor, **A1-NH$_2$** was coupled with aminoalkyl-Tra **11** by double amidation through a diglycolic acid spacer to produce **A1-L2^{25}-Tra**, in which the Akt inhibitor was connected to the linker via an amide bond. The longest linker in this study was prepared by "doubling" the linker length of L2, as described in the synthetic scheme for benzyl ester **15** prepared from **14** and **9**. Benzyl deprotection of **15** followed by amidation with **1** afforded aminoalkyl-Tra **17**. This intermediate was subsequently converted into **A1-L2^{42}-Tra** in three steps, similar to the synthesis of **A1-L2^{22}-Tra** from **11**.

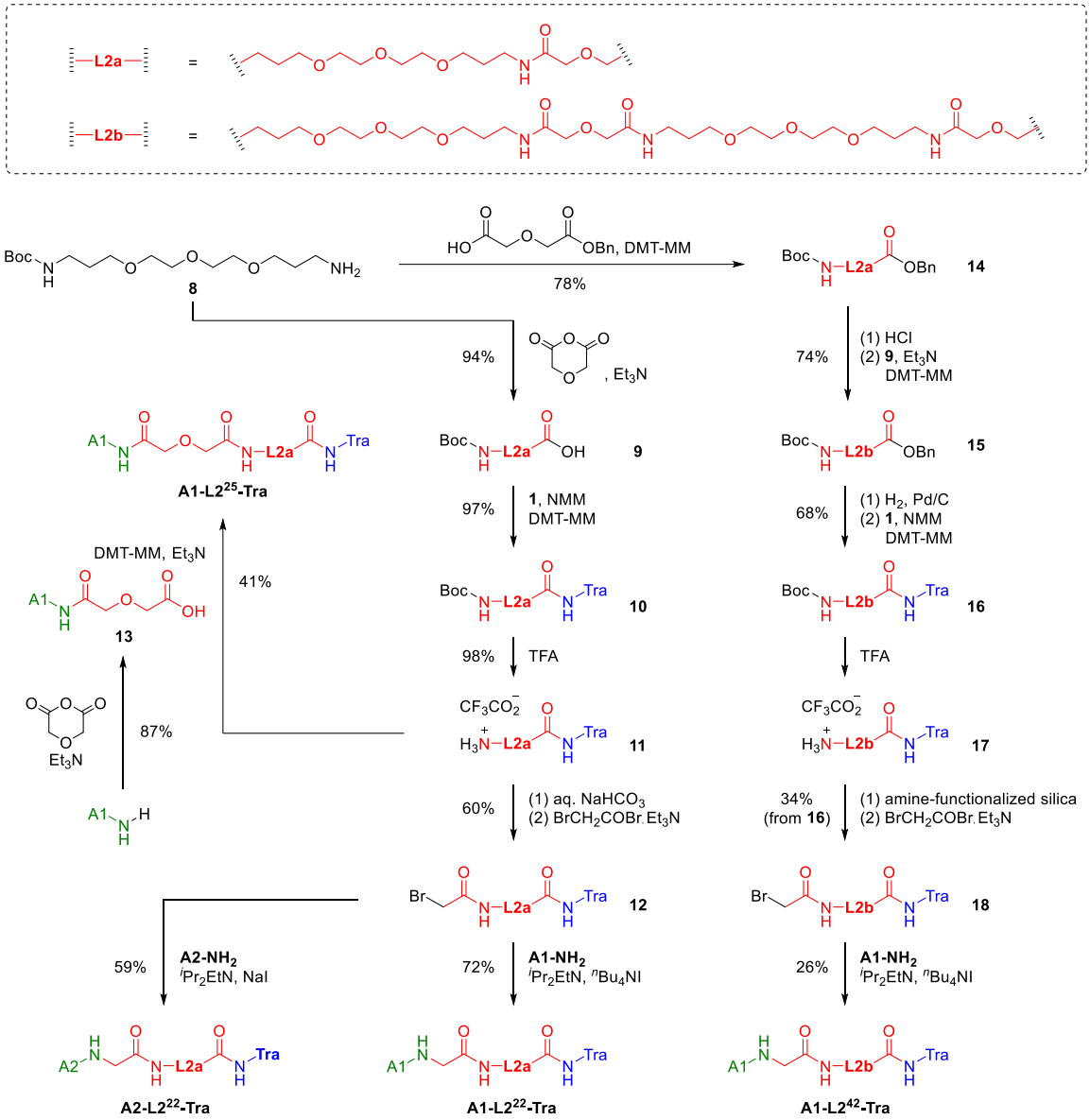

Scheme 2. Synthesis of four DDCs composed of an Akt inhibitor moiety (A1 or A2), linker L2 with a length of 22–42, and Tra.

Dipeptide-based linkers (L3) containing an aspartic acid (Asp) or histidine (His) residue were designed to explore linker structures with a chiral center and acid/base functionality (Scheme 3). Such dipeptide moieties might promote membrane penetration by being recognized by transporters.[32] Amidation of Fmoc-Asp(^{t}Bu)-OH (**19**) with **1** using DMT-MM afforded Tra conjugate **20** in 65% yield. Fmoc deprotection of **20**, followed by bromoacetylation, delivered the bromoalkyl-Tra intermediate **21** in 53% yield. The alkylative coupling of **21** with **A1-NH$_2$** followed by deprotection of the *t*-butyl group on the side chain, provided the Asp-residue containing DDC, **A1-L3^{5,Asp}-Tra**, in 35% yield (obtained as an HCl salt). Similarly, **A1-L3^{5,His}-Tra** containing a His residue in the linker, was synthesized from Fmoc-His(Boc)-OH (**22**) in five steps.

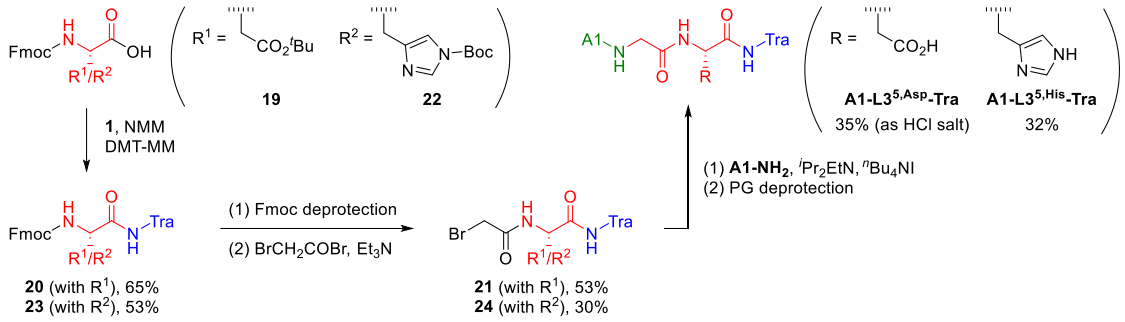

Scheme 3. Synthesis of two DDCs composed of Akt inhibitor moiety A1, linker L3 with a length of 5, and Tra.

Additionally, we prepared a DDC containing a fluorous linker (L4) because the fluorous effect of the perfluoroalkyl group in the linker could affect its physicochemical properties such as electrostatics, conformation, and interaction with proteins (Scheme 4).[33] Hydroxy-*t*-butyl ester **25** was converted to bromoalkyl-Tra **28** in six steps, which was then conjugated with **A1-NH$_2$** to afford **A1-L4^{16}-Tra** in 46% yield.

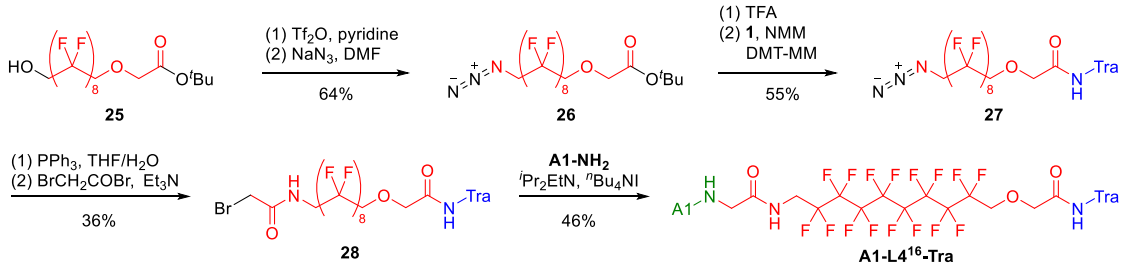

Scheme 4. Synthesis of a DDC composed of Akt inhibitor moiety A1, linker L4 with a length of 16, and Tra.

2.1.2. Inhibition of RAS-mutant cancer cell proliferation (H358)

The drugs and the synthesized DDCs were evaluated for antiproliferative activity using a RAS G12C-mutant lung cancer cell line H358 with treatment concentrations of 0.1, 1, and 10 μM (Fig. 2A). Trametinib exhibited approximately 60% inhibition activity at 0.1 μM. However, this activity had reached a plateau, resulting in no change in cell viability at higher concentrations. However, 80–90% inhibition was observed when **A1-NH$_2$** (which has a lower potency on its own) was used in combination with trametinib at the same concentration of 1–10 μM. This result indicated that trametinib requires the cooperation of an Akt inhibitor to achieve an inhibition well above 60%. Subsequently, we evaluated the first series of DDCs containing the Akt inhibitor moiety of either A1 or A2. This study aimed to identify the structural characteristics of DDCs necessary to achieve more than 60% inhibition, a level unattainable by trametinib alone, under the assay conditions employed. Among the four DDCs bearing the A1 moiety and linker L1, **A1-L1^6-Tra** yielded the most promising results. Notably, it achieved complete inhibition at 10 μM, although its inhibitory activity at 0.1–1 μM was lower than that of trametinib. **A1-L1^2-Tra**, **A1-L1^{10}-Tra**, and **A1-L1^{16}-Tra**, which possessed short or long L1, exhibited lower activity than **A1-L1^6-Tra**. These findings

suggest the existence of an optimal length for the linker L1. **A1-L2^{22}-Tra** demonstrated a high potency (approximately 90% inhibition) at 10 μM. However, when the linker was extended (**A1-L2^{42}-Tra**), inhibitory activity decreased. Furthermore, **A1-L2^{25}-Tra**, in which the A1 moiety was linked by an amide bond, exhibited lower activity than **A1-L2^{22}-Tra** did at a comparison of 1 μM (cell viability of 78.1 ± 2.7% vs. 58.3 ± 9.0%). Therefore, it can be inferred that the basic amino group in the A1 moiety has a favorable effect on the activity of **A1-L2^{22}-Tra**. The DDCs containing linkers L3 and L4 (**A1-L3^{5,Asp}-Tra**, **A1-L3^{5,His}-Tra**, and **A1-L4^{16}-Tra**) were not as potent as trametinib at all treatment concentrations. Comparable trends were observed when the Akt inhibitor was switched from **A1-NH$_2$** to similarly active **A2-NH$_2$**. The combined use of **A2-NH$_2$** and trametinib enhanced its activity. **A2-L1^{2}-Tra**, **A2-L1^{6}-Tra**, and **A2-L2^{22}-Tra** demonstrated concentration-dependent inhibitory effects similar to those of the corresponding DDCs with the A1 moiety. The two latter DDCs achieved >80% inhibition at 10 μM. These observations emphasize the significance of linker structure in DDC activity. Furthermore, compounds **7** and **11**, which lacked the Akt inhibitor moiety and possessed an amino group at the ends of linkers L1 and L2, respectively, did not attain over 80% inhibitory activity at any concentration. This indicates the significant role of the Akt inhibitor moiety in the corresponding DDCs (**A1/A2-L1^{6}-Tra** and **A1/A2-L2^{22}-Tra**, respectively).

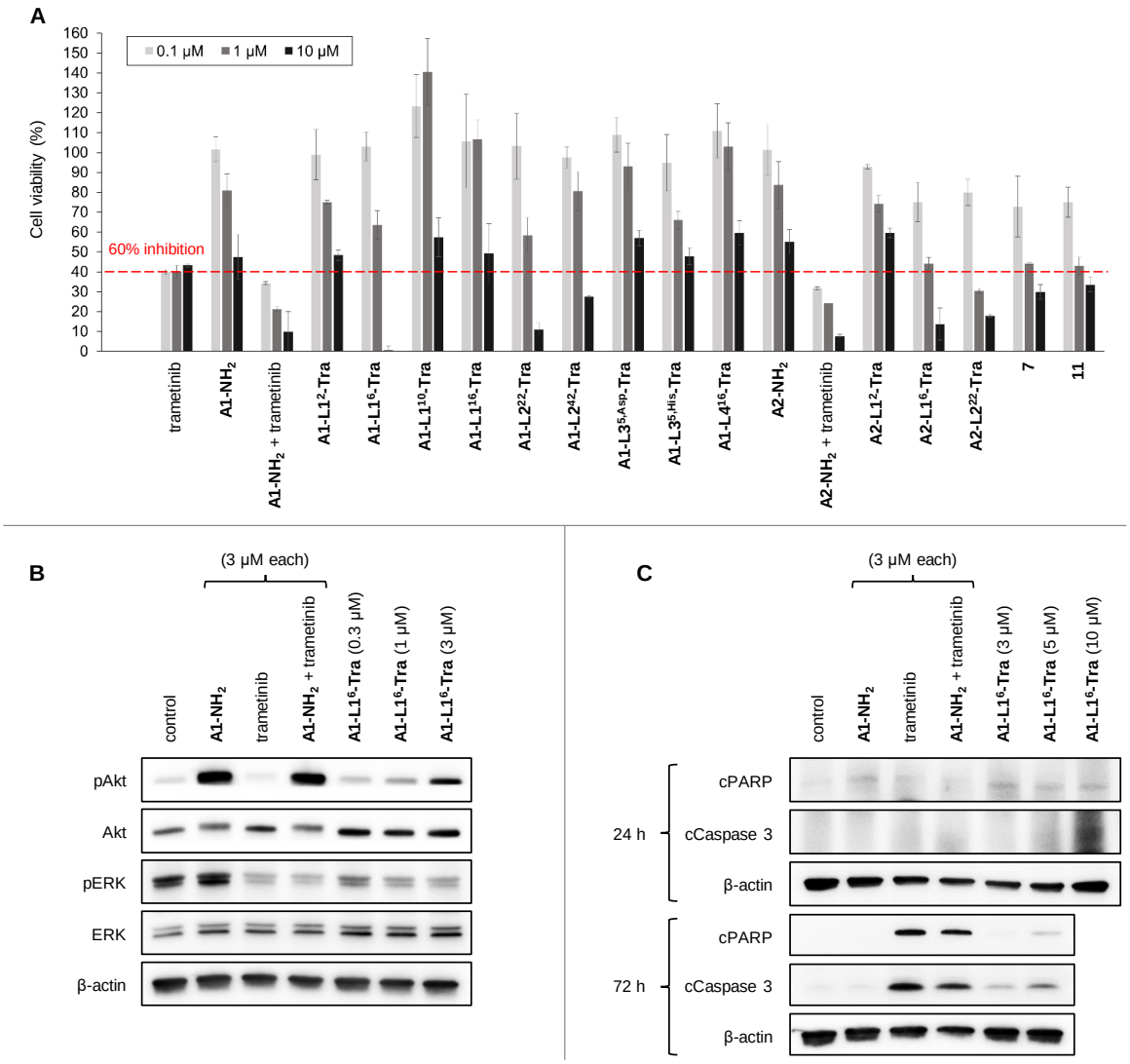

Fig. 2. *In vitro* evaluation of the anticancer activity of first-series DDCs. (A) RAS-mutant cancer cell proliferation inhibition. (B) Cell signaling pathway inhibition. (C) Detection of apoptosis-related proteins.

A1-L1^6-Tra demonstrated the most potent inhibitory effect among all the first-series DDCs at a concentration of 10 μM. Furthermore, this DDC can be easily synthesized from starting material **1** in two steps. Consequently, we designated **A1-L1^6-Tra** as the benchmark DDC for subsequent investigations.

2.1.3. Signal inhibition and induction of apoptosis-related proteins

We investigated the impact of **A1-L1^6-Tra** on signaling proteins in both the PI3K–Akt–mTOR and Raf–MEK–ERK pathways. Fig. 2B shows the Western blot analysis used to assess the Akt and ERK phosphorylation states 4 h after the treatment with **A1-NH$_2$**, trametinib, their combination, or **A1-L1^6-Tra**. **A1-NH$_2$** (3 μM) increased phosphorylated Akt (pAkt) via inhibitory binding to Akt,[8] while trametinib (3 μM) reduced phosphorylated ERK (pERK) by blocking the ERK phosphorylation.[14] The simultaneous use of these two drugs (3 μM each) provided combined results. **A1-L1^6-Tra** (3 μM) induced the pAkt accumulation and decreased pERK levels, albeit more vaguely apparent at lower concentrations (0.3 and 1

μM). Subsequent Western blot analysis was conducted to detect the apoptosis-related proteins cleaved PARP (cPARP) and cleaved caspase 3 (cCaspase 3) (Fig. 2C). No significant apoptosis-related proteins were observed at 24 h with the treatment of **A1-NH$_2$** (3 μM), trametinib (3 μM), their combination (3 μM each), or **A1-L1^6-Tra** (3–5 μM). However, cCaspase 3 was possibly generated with **A1-L1^6-Tra** treatment (10 μM). In contrast, both cPARP and cCaspase 3 were detected after 72 h of trametinib treatment, regardless of **A1-NH$_2$** presence. **A1-L1^6-Tra** (3 and 5 μM) dose-dependently induced cPARP and cCaspase 3 after 72 h, though not strongly. Taken together, the data depicted in Figs. 2B and 2C indicate that **A1-L1^6-Tra** displays inhibitory effects on both MEK and Akt and can induce sufficient apoptosis at a concentration of 5 μM.

2.1.4. Comparison of IC_{90}/IC_{50} ratios

The 5 μM concentration of **A1-L1^6-Tra** necessary to induce apoptosis (Fig. 2C) corresponds roughly to its IC_{90} (7.8 μM) obtained from the antiproliferative assay results (Fig. 2A). Therefore, the IC_{90} values of the DDCs could provide an approximate estimate of the DDC concentration that is capable of inducing apoptosis or cell death in H358 cells. Table 1 summarizes the IC_{90}/IC_{50} ratios, along with the IC_{50} and IC_{90} values of the four selected DDCs (**A1-L1^6-Tra**, **A1-L2^{22}-Tra**, **A2-L1^6-Tra**, and **A2-L2^{22}-Tra**) and drug combinations (trametinib with **A1-NH$_2$** or **A2-NH$_2$**). These DDCs have significantly lower IC_{90}/IC_{50} ratios (6.0–20, entries 1–4) compared to the drug combinations (>88, entries 5 and 6), indicating a superior ability of these DDCs to induce apoptosis or cell death, despite their moderate IC_{50} values (0.58–1.5 μM, entries 1–4).

Table 1

Summary of IC_{50}, IC_{90}, and IC_{90}/IC_{50} ratios for selected DDCs and drug combinations.

Entry	DDC or drugs	IC_{50}[a]	IC_{90}[a]	IC_{90}/IC_{50}
1	**A1-L1^6-Tra**	1.3	7.8	6.0
2	**A1-L2^{22}-Tra**	1.5	11	7.1
3	**A2-L1^6-Tra**	0.81	12	15
4	**A2-L2^{22}-Tra**	0.58	11	20
5	trametinib + **A1-NH$_2$**	<0.1	9.1	>91
6	trametinib + **A2-NH$_2$**	<0.1	8.8	>88

[a] Mean of more than two experiments.

2.1.5. Evaluation of cell permeability and intracellular accumulation

Since the accessibility of drug molecules to intracellular enzymes depends on their ability to migrate into cells, we investigated the cell permeability and the intracellular accumulation of the Akt inhibitors and the DDCs using cancer cells.[34] Akt inhibitors **A1-NH$_2$** and **A2-NH$_2$** exhibited sufficient cell permeability [the apparent permeability coefficients (P_{app}) of $8.55 \pm 0.87 \times 10^{-6}$ and $18.9 \pm 3.2 \times 10^{-6}$ cm/sec,

respectively, Fig. 3A] and accumulation values (cell to medium ratios) of 37.3 ± 0.3 and 34.5 ± 2.7 μL/cm^2, respectively (Fig. 3B). In contrast, the benchmark DDC, **A1-L1^6-Tra**, showed no detectable permeability and accumulated 7.5–8 times less (4.63 ± 0.38 μL/cm^2) than these Akt inhibitors. The A2 analog **A2-L1^6-Tra** displayed minimal permeability (P_{app} = 0.0984 ± 0.0348 × 10^{-6} cm/sec) and moderate accumulation (15.9 ± 2.9 μL/cm^2).

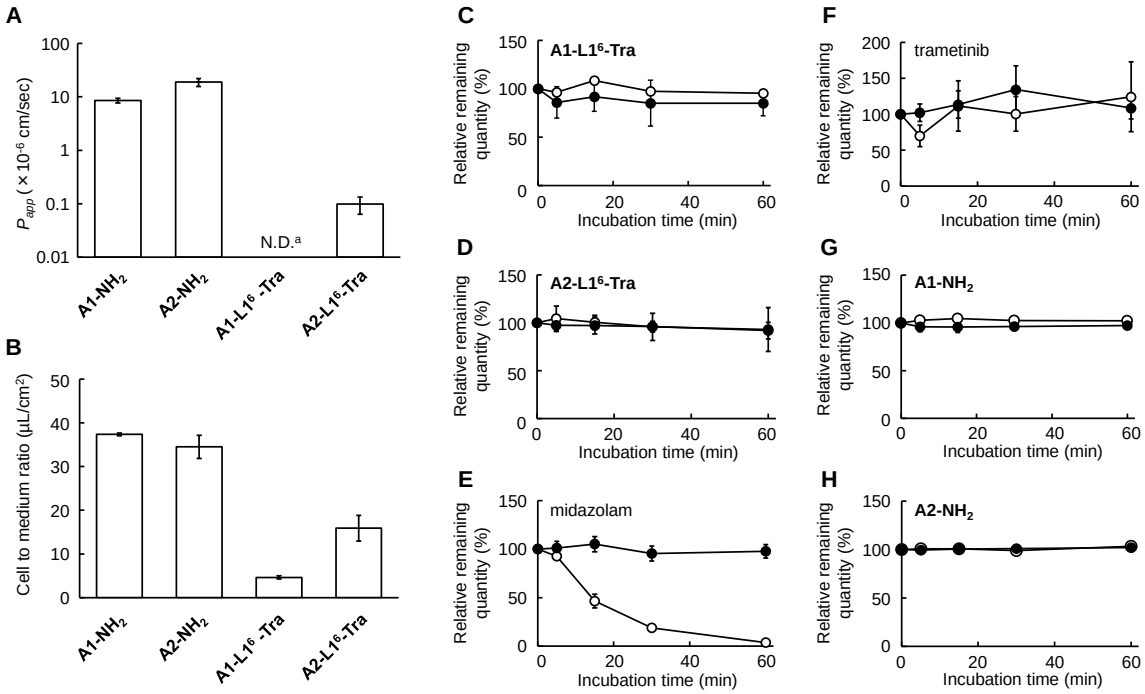

Fig. 3. *In vitro* characterization of **A1-L1^6-Tra** and **A2-L1^6-Tra**. (A) Comparison of cell permeability. [a] Not detected. (B) Comparison of intracellular accumulation. (C–H) Stability of hepatic metabolic enzymes. The experiments were conducted in the presence (empty circles) or absence (filled circles) of NADPH.

Table 2 shows the intracellular accumulation of the five selected DDCs containing linkers L1–L4 relative to **A1-L1^6-Tra** (entry 1). The low relative accumulation values (0.11–0.49) of **A1-L2^2-Tra** (entry 2), **A2-L2^2-Tra** (entry 3), **A1-L3^{5,His}-Tra** (entry 5), and **A1-L4^{16}-Tra** (entry 6) suggest their limited cell penetration ability, which can be responsible for their low antiproliferative activity even at 10 μM as shown in Fig. 2A.

Table 2

Relative intracellular accumulation of the first-series DDCs.

Entry	Linker class	DDC	Relative intracellular accumulation[a]
1	L1	**A1-L1^{6}-Tra**	1.0
2	L1	**A1-L2^{2}-Tra**	0.49
3	L1	**A2-L2^{2}-Tra**	0.35
4	L2	**A1-L2^{22}-Tra**	0.87
5	L3	**A1-L3^{5,His}-Tra**	0.11
6	L4	**A1-L4^{16}-Tra**	0.13

[a] Calculated using mean values of three experiments.

These data indicate that both the Akt inhibitor moiety and the linker structure influence cell permeability and intracellular DDC accumulation. Additionally, it has been suggested that the intracellular accessibility of DDCs must be improved to attain potent antiproliferative activity at low concentrations (0.1–1 μM).

2.1.6. Stability of hepatic metabolic enzymes

The stability of **A1-L1^{6}-Tra** and **A2-L1^{6}-Tra** to hepatic metabolic enzymes was examined in human liver microsomes. No significant degradation of these DDCs occurred within 60 min regardless of NADPH presence (Fig. 3C and D). In contrast, midazolam, a CYP3A substrate, was almost entirely degraded in the presence of NADPH (Fig. 3E). Moreover, the sufficient stabilities of trametinib, **A1-NH$_2$**, and **A2-NH$_2$** were confirmed under these conditions (Fig. 3F–H). Thus, conjugation of trametinib and Akt inhibitors with linker L1^{6} did not cause metabolic susceptibility.

2.2. Synthesis and in vitro characterization of the second-series DDCs

2.2.1. Design and synthesis

Based on the evaluation results of the first series of DDCs, 12 additional DDCs were designed and synthesized to achieve enhanced activity. For the second series of DDCs, two pyrrolopyrimidine-based Akt inhibitors, **A3-NH$_2$** (Akt2 IC$_{50}$ = 180 nM)[35] and **A4-NH** (Akt1 IC$_{50}$ = 4 nM),[36] were employed (Scheme 5). Because of the lower molecular weights of **A3-NH$_2$** (217) and **A4-NH** (292) compared to those of **A1-NH$_2$** (405) and **A2-NH$_2$** (407), we expected that A3- or A4-containing DDCs would have improved accessibility to intracellular MEK proteins. We synthesized **A3-L1^{6}-Tra** and **A4-L1^{6}-Tra**, which are A3 and A4 analogs of the benchmark **A1-L1^{6}-Tra**, by the alkylative coupling of **3** with **A3-NH$_2$** and **A4-NH**, respectively, in 49–50% yield. In addition, three DDCs containing oxyethylene linkers (L5) with lengths of 6–9 were synthesized as the oxa analogs of **A4-L1^{6}-Tra** (Scheme 6). Linker L5 is structurally similar to the linker contained in a trametinib-based probe that was used to study the complexation between MEK and KSR.[28]

Carboxylic acid ^{t}Bu esters **29**–**31** bearing a tosylate LG were converted to **A4-L5^6-Tra**, **A4-L5^8-Tra**, and **A4-L5^9-Tra**, respectively, by the three-step reactions of ^{t}Bu group deprotection, amidation with **1**, and the alkylative coupling with **A4-NH**.

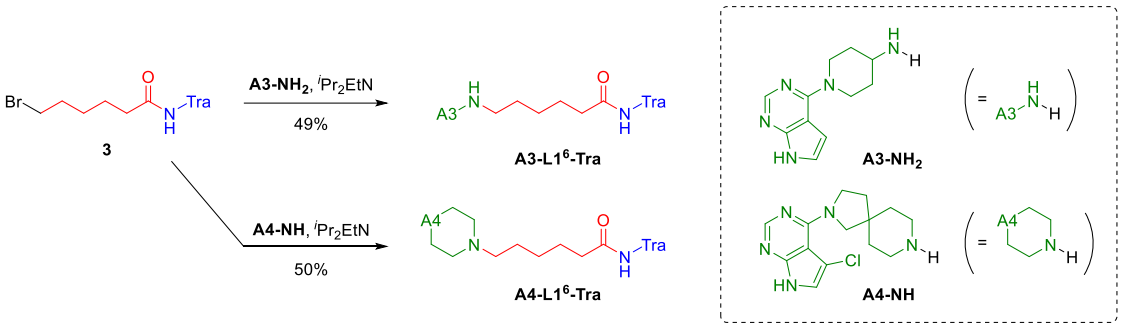

Scheme 5. Synthesis of two DDCs composed of an Akt inhibitor moiety (A3 or A4), linker L1 with a length of 6, and Tra.

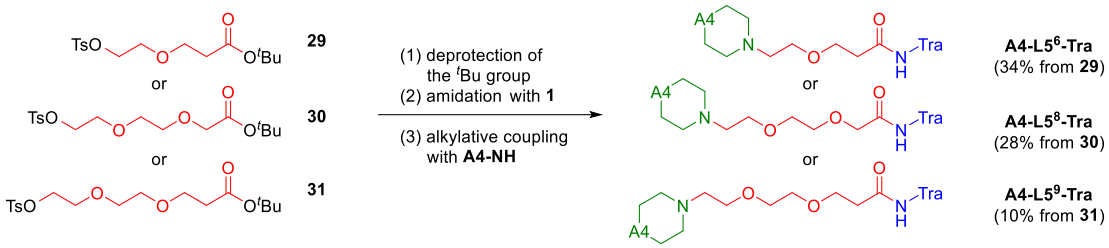

Scheme 6. Synthesis of three DDCs composed of Akt inhibitor moiety A4, linker L5 with a length of 6–9, and Tra.

The use of a linker with an embedded heteroaromatic ring may improve the DDC activity. This is because structurally rigid linkers can facilitate the spatial separation of the Tra and Akt inhibitor moieties to suppress their possible inactivation by self-aggregation. Therefore, furan- and 1,3,5-triazine-containing linkers (L6 and L7 with lengths of 9 and 7, Schemes 7 and 8, respectively) were employed for DDC synthesis. Linker L6 was originally developed to study the conformation and reactivity of oligo(acetylacetone)s.[37] 1,3,5-Triazines have been used as polymer backbones and hub molecules because they can rapidly assemble multiple functionalities via aromatic nucleophilic substitution at the triazine core.[38,39] Symmetric dibromo compound **32** (Scheme 7) was sequentially coupled with **1** (57% yield) and the four Akt inhibitors (9–68% yield) to afford **A1-L6^9-Tra**, **A2-L6^9-Tra**, **A3-L6^9-Tra**, and **A4-L6^9-Tra**. Both Tra and Akt inhibitor moieties were attached to the linker via alkylation. DDCs with linker L7 were synthesized from 1,3,5-triazine **34** bearing chloro and (3-chloro)propoxy groups (Scheme 8). *N*-Triazinylation of the aromatic amino group of **1** with **34** afforded the chloroalkyl-Tra intermediate **35**, which was coupled with **A1-NH$_2$**, **A2-NH$_2$**, and **A4-NH** to afford **A1-L7^7-Tra**, **A2-L7^7-Tra**, and **A4-L7^7-Tra**, respectively, in 6–24% yield.

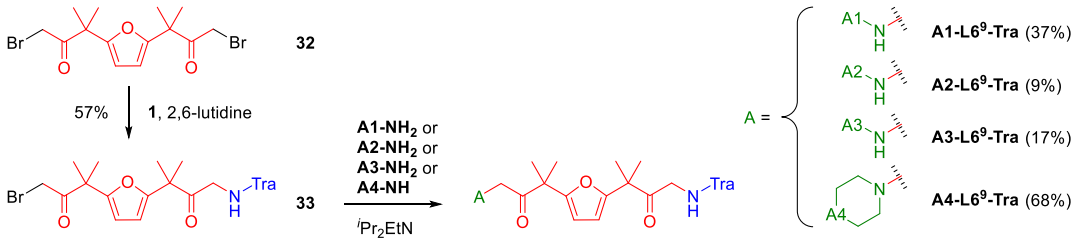

Scheme 7. Synthesis of four DDCs composed of an Akt inhibitor moiety (A1, A2, A3, or A4), linker L6 with a length of 9, and Tra.

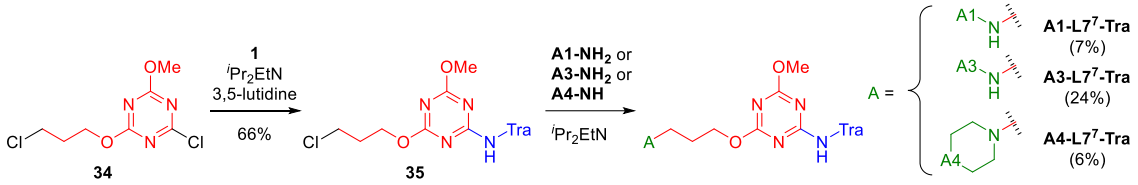

Scheme 8. Synthesis of three DDCs composed of an Akt inhibitor moiety (A1, A3, or A4), linker L7 with a length of 7, and Tra.

2.2.2. Evaluation of intracellular accumulation

Table 3 describes the intracellular accumulation values of the second-series DDCs relative to **A1-L1^6-Tra** (entry 1). The accumulation increased by a factor of 9.5 and 3.5 when the A1 moiety in **A1-L1^6-Tra** was substituted with the A3 and the A4 moieties, respectively (entry 1 vs. entries 2 and 3). Replacing the linker L1^6 in **A4-L1^6-Tra** (entry 3) with linkers L5^6, L5^8, and L5^9 maintained the improved accumulation (3.3–7.4, entries 4–6). In contrast, **A2-L6^9-Tra**, **A3-L6^9-Tra**, and **A4-L6^9-Tra** exhibited lower accumulation (0.55–1.4, entries 7–9) regardless of the Akt inhibitor moiety. However, among the DDCs containing L7, **A3-L7^7-Tra** showed a higher accumulation (5.9, entry 11) than **A1-L7^7-Tra** (0.86, entry 10) and **A4-L7^7-Tra** (0.24, entry 12). The results in Table 3 suggest that the small Akt inhibitor moiety (A3<A4<A1 and A2) and the structurally simple linker (L1^6 and L5$^{6–9}$ instead of L6^9 and L7^7) tended to enhance intracellular accumulation.

Table 3

Relative intracellular accumulation of the second-series DDCs.

Entry	Linker class	DDC	Relative intracellular accumulation[a]
1	L1	**A1-L1^{6}-Tra**	1.0
2	L1	**A3-L1^{6}-Tra**	9.5
3	L1	**A4-L1^{6}-Tra**	3.5
4	L5	**A4-L5^{6}-Tra**	6.6
5	L5	**A4-L5^{8}-Tra**	3.3
6	L5	**A4-L5^{9}-Tra**	7.4
7	L6	**A2-L6^{9}-Tra**	1.4
8	L6	**A3-L6^{9}-Tra**	1.2
9	L6	**A4-L6^{9}-Tra**	0.55
10	L7	**A1-L7^{7}-Tra**	0.86
11	L7	**A3-L7^{7}-Tra**	5.9
12	L7	**A4-L7^{7}-Tra**	0.24

[a] Calculated using mean values of three experiments.

2.2.3. Inhibition of RAS-mutant cancer cell proliferation (H358)

The antiproliferative activity of the second-series DDCs was evaluated using H358 cells (Table 4). The IC_{50} of **A1-L1^{6}-Tra** (1.3 μM, entry 1) was enhanced in **A3-L1^{6}-Tra** (0.098 μM, entry 2) and further improved in **A4-L1^{6}-Tra** (0.017 μM, entry 3). When the linker structure was slightly modified in **A4-L1^{6}-Tra**, specifically the CH_2–O exchange in the middle of the linker, resulting in **A4-L5^{6}-Tra**, caused a decrease in inhibitory activity (0.20 μM, entry 4). Interestingly, extending the L5 linker length from 6 to 8 and 9 has resulted in the recovery of the activity (0.013 and 0.044 μM, entries 5 and 6). These improved IC_{50} values (entries 1 vs. 2–6) can be interpreted based on the importance of DDC accessibility to intracellular enzymes rather than the Akt inhibitor potency. The DDCs containing linker L6 (**A1-L6^{9}-Tra**, **A2-L6^{9}-Tra**, **A3-L6^{9}-Tra**, and **A4-L6^{9}-Tra**) exhibited remarkably strong activity (0.0039–0.077 μM, entries 7–10), despite their low ability to accumulate in cells. The activity of DDCs containing linker L7 depended on their Akt inhibitor moiety (**A1-L7^{7}-Tra**, 1.0 μM, entry 11; **A3-L7^{7}-Tra**, 0.079 μM. Entry 12; and **A4-L7^{7}-Tra**, 0.40 μM, entry 13). Although the effects of linkers L6 and L7 on the DDC activity are noteworthy, their origin remains unclear.

Table 4

Antiproliferative activity of the second-series DDCs.

Entry	Linker class	DDC	IC_{50} (μM)[a]	
			H358	HCT116
1	L1	**A1-L1^{6}-Tra**	1.3	0.34
2	L1	**A3-L1^{6}-Tra**	0.098	0.31
3	L1	**A4-L1^{6}-Tra**	0.017	0.043
4	L5	**A4-L5^{6}-Tra**	0.20	0.31
5	L5	**A4-L5^{8}-Tra**	0.013	0.039
6	L5	**A4-L5^{9}-Tra**	0.044	0.033
7	L6	**A1-L6^{9}-Tra**	0.0058	0.0038
8	L6	**A2-L6^{9}-Tra**	0.077	0.053
9	L6	**A3-L6^{9}-Tra**	0.014	0.0038
10	L6	**A4-L6^{9}-Tra**	0.0039	0.0051
11	L7	**A1-L7^{7}-Tra**	1.0	0.025
12	L7	**A3-L7^{7}-Tra**	0.079	0.054
13	L7	**A4-L7^{7}-Tra**	0.40	0.012

[a] Mean of more than two experiments.

2.2.4. Inhibition of RAS-mutant cancer cell proliferation (HCT116)

Table 4 shows the antiproliferative assay results of the second-series DDCs using another RAS-mutant cell line, HCT116, a colorectal cancer cell line with the RAS G13D-mutation (see Table S1 for the corresponding assay of the first-series DDCs). Similar to the assay results using H358 cells, all second-series DDCs exhibited lower IC_{50} values than the benchmark **A1-L1^{6}-Tra**. The DDCs from the L5, L6, and L7 series with appropriate linker lengths demonstrated inhibitory activity over 10 times higher than those of **A1-L1^{6}-Tra**. Especially, **A1-L6^{9}-Tra** (entry 7), **A3-L6^{9}-Tra** (entry 9), and **A4-L6^{9}-Tra** (entry 10) exhibited strong activity (IC_{50} values of 0.0038–0.0051 μM), indicating their promising properties as the DDCs for treating RAS-mutant cancers.

3. *In vivo* characterization of selected DDCs

Preliminary *in vivo* studies were conducted on **A1-L1^{6}-Tra** (the benchmark DDC) and **A1-L6^{9}-Tra** (one of the most potent DDCs; Table 4) to examine their PK characteristics and anticancer efficacy.

3.1. PK characteristics in mice

The PK characteristics of trametinib, **A1-NH$_2$**, and the two DDCs were evaluated in mice after subcutaneous (sc) administration. Trametinib exhibited a long blood half-life of 12.4 h (Fig. 4A) owing to its sustained binding to MEK,[26,27] which was 3.9 times greater than that of **A1-NH$_2$** (3.2 h, Fig. 4B). The half-lives of **A1-L1^6-Tra** (19.3 h, Fig. 4C) and **A1-L6^9-Tra** (6.1 h, Fig. 4D) were 1.9–6.0 times longer than that of **A1-NH$_2$**. Given their durability, **A1-L1^6-Tra** and **A1-L6^9-Tra** remained in the blood for up to 25 h (at concentrations of 11 and 5.2 nM, respectively) after 1 mg/kg doses were administered. Therefore, trametinib conjugation extended the half-life of **A1-NH$_2$**, depending on the linker structure of the DDCs. It is noteworthy that the PK profiles of trametinib and **A1-NH$_2$** differed significantly, which presents a challenge when using them in combination therapies. In contrast, **A1-L1^6-Tra** and **A1-L6^9-Tra** successfully unified the PK profiles of trametinib and **A1-NH$_2$** through the DDC formation.

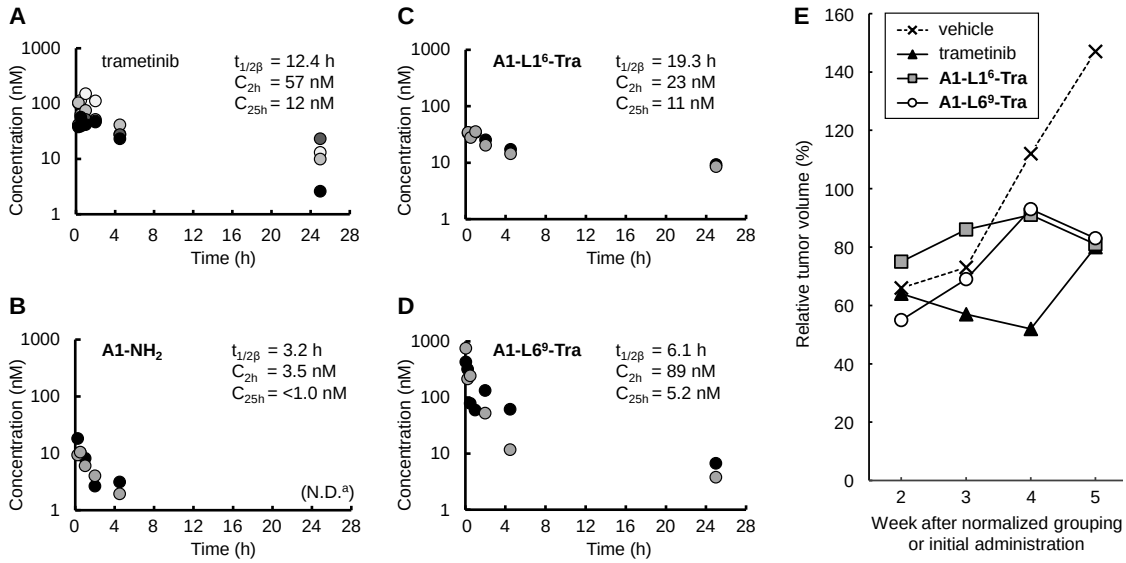

Fig. 4. *In vivo* evaluation of **A1-L1^6-Tra** and **A1-L6^9-Tra**. (A–D) Comparison of PK characteristics in mice. [a] Concentration of **A1-NH$_2$** at 25 h was lower than the detection limit (1.0 nM). (E) Anticancer efficacy in mice grafted with H358.

3.2. Anticancer efficacies of selected DDCs and trametinib in mice grafted with H358

The anticancer efficacies of **A1-L1^6-Tra** and **A1-L6^9-Tra** were compared to that of trametinib in mice bearing H358 grafts (Fig. 4E). The sc administration was performed three times a week at a dose of 1.0 μmol/kg. At week 4, trametinib effectively reduced cancer cells; however, these DDCs did not show a significant response. However, at week 5, the anticancer efficacies of all compounds examined were comparable.

4. Conclusion

We conjugated trametinib and Akt inhibitors using various linkers to synthesize novel DDCs for the concurrent and sustained Raf–MEK–ERK and PI3K–Akt–mTOR signaling pathway blocking. The first-series DDCs (13 in total) contained afuresertib or MK2206 as the Akt inhibitor moiety and a linker with

aliphatic chain, oxyethylene-amide, dipeptide, and fluorous structures. Signal inhibition, apoptosis-inducing ability, and sufficient stability of hepatic metabolic enzymes were confirmed for **A1-L1^6-Tra**, which was used as the benchmark DDC throughout this study. The antiproliferative activity of the first-series DDCs against RAS-mutant cancer cell lines was successfully improved in the second series (12 in total), which additionally employed pyrrolopyrimidine-based Akt inhibitors and linkers containing oxyethylene, furan, and 1,3,5-triazine structures. Among them, **A1-L6^9-Tra** and **A4-L6^9-Tra** containing the furan-based linker, were identified as the most potent DDCs in the *in vitro* assay. Preliminary *in vivo* studies using **A1-L1^6-Tra** and **A1-L6^9-Tra** demonstrated that their half-lives in mice were prolonged compared to **A1-NH$_2$** due to trametinib conjugation, as expected from our molecular design. The DDC formation unified the PK profiles of trametinib and **A1-NH$_2$**. **A1-L1^6-Tra** and **A1-L6^9-Tra** demonstrated anticancer efficacies comparable to those of trametinib in mice grafted with H358 cells. Collectively, the DDC-based strategy described in this study is potentially attractive for treating RAS-mutant cancers. Further investigation of the second-series DDCs, including an *in vitro* assay to evaluate their apoptosis-inducing ability and detailed *in vivo* studies, is currently in progress.

5. Material and methods

5.1. In vitro experiments

5.1.1. Antiproliferative assay for the first-series DDCs

Cell viability was measured by the MTT assay.[40] H358 cells were seeded in RPMI 1640 medium (supplemented with 10% fetal bovine serum) in 96-well plates at a density of 3×10^3 cells/100 μL per well and were incubated for 24 h. The test compounds (100 μL, a final concentration of 0.1–10 μM in the medium containing <0.2% DMSO) were then added to each well and the cells were incubated for an additional 3 d. After adding the MTT solution (2 mg/mL), the cells were incubated for 2 h. After removing the medium containing MTT, the residue remaining in each well was dissolved in DMSO (50 μL). The absorbance at 570 nm was measured using a microplate reader (iMark, Bio-Rad Laboratories, Hercules, CA, USA). The cell viability percentage was calculated by comparison with the untreated control samples. IC_{50} values were determined by fitting the inhibition curves using regression analysis.

5.1.2. Western blot analysis

Protein aliquots (15 μg) were separated by SDS-PAGE using an electrophoresis system (Bio-Rad Laboratories) and transferred to polyvinylidene difluoride membranes (Bio-Rad Laboratories). The membranes were washed thrice and incubated with a Blocking Buffer (Thermo Fisher Scientific, Waltham, MA, USA) for 1 h at room temperature. The membranes were incubated overnight at 4 °C with primary antibodies. The membranes were washed thrice and incubated for 1 h at room temperature with species-specific horseradish peroxidase-conjugated secondary antibodies. Immunoreactive bands were visualized using Immobilon Western Chemiluminescent HRP Substrate (Merck). Antibodies against pAkt (Ser473), Akt, phosphorylated p42/44 MAP kinase (Thr202/Tyr204), p42/44 MAP kinase, cPARP, cCaspase 3, and β-actin were purchased from Cell Signaling Technology (Danvers, MA, USA).

5.1.3. Antiproliferative assay for the second-series DDCs

Cell viability was measured using the WST-8 assay with Cell Count Reagent SF (Nacalai Tesque, Tokyo, Japan). The procedure was established according to the previous reports.[14,16] In brief, H358 or HCT116 cells were seeded in 96-well plates at a density of 2.5×10^3 cells/100 μL per well and were incubated for approximately 3 d until they reached less than 30% confluency. The test compounds (100 μL, dissolved in the medium containing <0.2% DMSO) were then added to each well, and the cells were incubated for an additional 3 d. Viable cells in each well were evaluated by adding the cell-counting reagent for the last 2.5–4 h. Absorbance was measured using a microplate reader (iMark) at 450 and 570 nm for the test and reference wavelengths, respectively. The cell viability percentage was calculated by comparison with the untreated control samples. IC_{50} values were determined by fitting the inhibition curves using regression analysis.

5.1.4. Metabolic stability study

The stability of hepatic metabolic enzymes was determined using pooled human liver microsomes (50 specimens; BD Gentest, Woburn, MA, USA). A master mix was prepared with potassium phosphate buffer (at a final concentration of 100 mM), $MgCl_2$ (at 10 mM), human liver microsomes (at 0.2 mg/mL), the test compound (at 10 μM), and midazolam (0 or 1 μM). After preincubation of the master mix (180 μL) for 5 min at 37 °C, 20 μL of the NADPH-generating system (comprising a final concentration of 5 mM glucose-6-phosphate, 0.5 mM β-$NADP^+$, 5 mM $MgCl_2$, and 1 unit/mL G6PDH) or purified water was added to initiate the reaction. After a designated time (0, 5, 15, 30, or 60 min), the reaction mixture (20 μL) was collected and diluted with ice-cold MeCN (20 μL) to quench the reaction. The residual test compound concentrations were measured using LC-MS/MS.

5.1.5. Cell permeability and cell accumulation study

The cell permeability was evaluated as described in the literature.[34] LLC-PK1 cells were cultured in Dulbecco's modified Eagle's medium containing 10 v/v% fetal bovine serum (Thermo Fisher Scientific), 100 units/mL penicillin, 100 μg/mL streptomycin, and 1 v/v% non-essential amino acids at 5% CO_2 and 37 °C. The cells were seeded in a 12-well plate at a density of 3.6×10^5 cells/cm^2 on cell culture inserts (Corning, Corning, NY, USA) and cultured for 6 d. The medium was replaced with fresh medium every 2 d. For transport studies, the cells were preincubated with an antibiotic-free culture medium for 10 min at 37 °C. The transport reaction was initiated by replacing the medium with an antibiotic-free culture medium containing the test compounds on the cell culture insert (donor side). After incubating for the designated time (0, 30, 60, 90, 120, or 180 min) at 37 °C, the medium (100 μL) was collected from the bottom dish (receiver side) and diluted with antibiotic-free medium (100 μL). To measure the intracellular accumulation of the test compounds, the cell culture inserts were washed with ice-cold PBS after the reaction. The cellular contents were extracted with the 1:1:2 mixture (80 μL) comprising antibiotic-free medium, 0.4 v/v% aqueous formic acid, and MeCN containing imatinib as an internal standard. The concentration of compounds was measured by LC-MS/MS. Uptake was expressed as the cell-to-medium ratio, which was calculated by dividing the

cellular uptake by the test compound concentration in the uptake medium. P_{app} was calculated using the following equation: $P_{app} = (dQ/dt)/(A \times C_0)$, where dQ/dt, A, and C_0 are the amount of the test compound transported over time t, the membrane surface area (0.9 cm^2), and the initial test compound concentration in the donor compartment, respectively.

5.2. In vivo experiments

5.2.1. PK analysis

After sc administration of test compounds (1 mg/kg, 100 uL/20 g mouse) into the back of mice, the blood samples were collected at the designated time (0.25, 0.5, 1, 2, 4, or 25 h). Blood samples were treated with 1/20 volume of ethylenediaminetetraacetic acid solution (15% in saline) and centrifuged (KOKUSAN, Tokyo, Japan) at 3000 rpm for 10 min. Plasma was separated and stored as frozen samples until the test compounds were quantified using LC-MS/MS. The half-lives ($T_{1/2}$) of the test compounds were calculated using the MOMENT program.[41]

5.2.2. Anticancer effect

A suspension of H358 cells (5×10^6) in Matrigel (Corning) was injected subcutaneously into the flanks of 6–8-week-old male nude mice (CLEA Japan, Tokyo, Japan). The care and treatment of the experimental animals were per the institutional guidelines. The injected tumor volumes in the mice were randomized (n = 8) when the mean volume exceeded 100 mm^3. A test compound solution (100 µL/20 g mouse) was administered subcutaneously into the back thrice a week. The test compounds were dissolved in a PBS buffer (containing 2% DMSO and 1% Tween 20) at a dosage of 1 µmol/kg. The mice were monitored thrice a week for body weight and general condition. The tumors were measured once a week using calipers. The tumor volume was calculated using the following formula: length × $width^2$ × 0.52. Per the institutional guidelines, the mice were sacrificed when their tumor volume reached 1,000 mm^3. Data were collected and the averages of n = 6 were calculated without the upper and lower tumor volumes in each group.

5.3. LC-MS/MS methods

The concentrations of test compounds were measured by LC-MS/MS (LCMS-8050, Shimadzu, Kyoto, Japan) coupled with an LC-30A system (Shimadzu). The analytical column was a CAPCELL PAK C18 (2.0 mm inner diameter × 50 mm, 3 µm, Osaka Soda, Osaka, Japan) maintained at 40 °C. The mobile phase consisted of 0.1% (v/v) aqueous formic acid (solvent A) and 0.1% (v/v) formic acid in MeCN (solvent B). The gradient compositions were as follows: 5% B (0–1 min), 5–80% B (1–2.5 min), 80% B (2.5–4.5 min), 80–5% B (4.5–5 min), and 5% B (5–8 min). The mobile phase flow rate and the sample injection volume were 0.4 mL/min and 3 µL, respectively. The mass transitions of the test compounds were monitored at the corresponding m/z values, as shown in Table S2. LabSolutions software (Shimadzu) was used for data manipulation. The lower detection limit was 1–10 nM for each test compound.

Declaration of Competing Interest

The authors declare that they have no competing financial interests or personal relationships that may have influenced the work reported in this study.

Data availability

Data will be made available on request.

Acknowledgment

This work was partly supported by the Japan Agency for Medical Research and Development (AMED) Grant Nos. 19lm023002j003, 20lm0203002j0004, and 21lm0203002j0005.

Supplementary data

Supplementary data to this article can be found online.

References

1. Prior IA, Hood FE, Hartley JL. The Frequency of Ras Mutations in Cancer. *Cancer Res*. 2020;80:2969–2974. doi:10.1158/0008-5472.CAN-19-3682
2. Sanchez-Vega F, Mina M, Armenia J, et al. Oncogenic Signaling Pathways in The Cancer Genome Atlas. *Cell*. 2018;173:321–337.e10. doi:10.1016/j.cell.2018.03.035
3. Mullard A. Amgen overcomes historically undruggable target, with FDA nod for first KRAS inhibitor. *Nat Rev Drug Discov*. 2021;20:496–496. doi:10.1038/d41573-021-00098-4
4. Moore AR, Malek S. The promise and peril of KRAS G12C inhibitors. *Cancer Cell*. 2021;39:1059–1061. doi:10.1016/j.ccell.2021.07.011
5. Feng S, Callow MG, Fortin J-P, et al. A saturation mutagenesis screen uncovers resistant and sensitizing secondary *KRAS* mutations to clinical $KRAS^{G12C}$ inhibitors. *Proc Natl Acad Sci*. 2022;119:1–7. doi:10.1073/pnas.2120512119
6. Wang X, Allen S, Blake JF, et al. Identification of MRTX1133, a Noncovalent, Potent, and Selective $KRAS^{G12D}$ Inhibitor. *J Med Chem*. 2022;65:3123–3133. doi:10.1021/acs.jmedchem.1c01688
7. Renshaw J, Taylor KR, Bishop R, et al. Dual Blockade of the PI3K/AKT/mTOR (AZD8055) and RAS/MEK/ERK (AZD6244) Pathways Synergistically Inhibits Rhabdomyosarcoma Cell Growth *In Vitro* and *In Vivo*. *Clin Cancer Res*. 2013;19:5940–5951. doi:10.1158/1078-0432.CCR-13-0850
8. Dumble M, Crouthamel M-C, Zhang S-Y, et al. Discovery of Novel AKT Inhibitors with Enhanced Anti-Tumor Effects in Combination with the MEK Inhibitor. *PLoS One*. 2014;9:e100880. doi:10.1371/journal.pone.0100880
9. Weisner J, Landel I, Reintjes C, et al. Preclinical Efficacy of Covalent-Allosteric AKT Inhibitor Borussertib in Combination with Trametinib in *KRAS*-Mutant Pancreatic and Colorectal Cancer. *Cancer Res*. 2019;79:2367–2378. doi:10.1158/0008-5472.CAN-18-2861

10. Molina-Arcas M, Moore C, Rana S, et al. Development of combination therapies to maximize the impact of KRAS-G12C inhibitors in lung cancer. *Sci Transl Med*. 2019;11. doi:10.1126/scitranslmed.aaw7999
11. Tolcher AW, Patnaik A, Papadopoulos KP, et al. Phase I study of the MEK inhibitor trametinib in combination with the AKT inhibitor afuresertib in patients with solid tumors and multiple myeloma. *Cancer Chemother Pharmacol*. 2015;75:183–189. doi:10.1007/s00280-014-2615-5
12. Tolcher AW, Kurzrock R, Valero V, et al. Phase I dose-escalation trial of the oral AKT inhibitor uprosertib in combination with the oral MEK1/MEK2 inhibitor trametinib in patients with solid tumors. *Cancer Chemother Pharmacol*. 2020;85:673–683. doi:10.1007/s00280-020-04038-8
13. Halilovic E, She Q-B, Ye Q, et al. PIK3CA Mutation Uncouples Tumor Growth and Cyclin D1 Regulation from MEK/ERK and Mutant KRAS Signaling. *Cancer Res*. 2010;70:6804–6814. doi:10.1158/0008-5472.CAN-10-0409
14. Kitai H, Ebi H, Tomida S, et al. Epithelial-to-Mesenchymal Transition Defines Feedback Activation of Receptor Tyrosine Kinase Signaling Induced by MEK Inhibition in *KRAS*-Mutant Lung Cancer. *Cancer Discov*. 2016;6:754–769. doi:10.1158/2159-8290.CD-15-1377
15. Balakirouchenane D, Guégan S, Csajka C, et al. Population Pharmacokinetics/Pharmacodynamics of Dabrafenib Plus Trametinib in Patients with BRAF-Mutated Metastatic Melanoma. *Cancers*. 2020;12:931. doi:10.3390/cancers12040931
16. Gilmartin AG, Bleam MR, Groy A, et al. GSK1120212 (JTP-74057) Is an Inhibitor of MEK Activity and Activation with Favorable Pharmacokinetic Properties for Sustained *In Vivo* Pathway Inhibition. *Clin Cancer Res*. 2011;17:989–1000. doi:10.1158/1078-0432.CCR-10-2200
17. Rodier T, Puszkiel A, Cardoso E, et al. Exposure–Response Analysis of Osimertinib in Patients with Advanced Non-Small-Cell Lung Cancer. *Pharmaceutics*. 2022;14:1844. doi:10.3390/pharmaceutics14091844
18. Raghavendra NM, Pingili D, Kadasi S, Mettu A, Prasad SVUM. Dual or multi-targeting inhibitors: The next generation anticancer agents. *Eur J Med Chem*. 2018;143:1277–1300. doi:10.1016/j.ejmech.2017.10.021
19. Hasan M, Leak RK, Stratford RE, Zlotos DP, Witt-Enderby PA. Drug conjugates—an emerging approach to treat breast cancer. *Pharmacol Res Perspect*. 2018;6. doi:10.1002/prp2.417
20. Szumilak M, Wiktorowska-Owczarek A, Stanczak A. Hybrid Drugs—A Strategy for Overcoming Anticancer Drug Resistance? *Molecules*. 2021;26:2601. doi:10.3390/molecules26092601
21. Wang Y, Tortorella M. Molecular design of dual inhibitors of PI3K and potential molecular target of cancer for its treatment: A review. *Eur J Med Chem*. 2022;228:114039. doi:10.1016/j.ejmech.2021.114039
22. Van Dort ME, Galbán S, Wang H, et al. Dual inhibition of allosteric mitogen-activated protein kinase (MEK) and phosphatidylinositol 3-kinase (PI3K) oncogenic targets with a bifunctional inhibitor. *Bioorg Med Chem*. 2015;23:1386–1394. doi:10.1016/j.bmc.2015.02.053
23. Rychahou PG, Kang J, Gulhati P, et al. Akt2 overexpression plays a critical role in the

establishment of colorectal cancer metastasis. *Proc Natl Acad Sci*. 2008;105:20315–20320. doi:10.1073/pnas.0810715105

24. Freeman-Cook KD, Autry C, Borzillo G, et al. Design of Selective, ATP-Competitive Inhibitors of Akt. *J Med Chem*. 2010;53:4615–4622. doi:10.1021/jm1003842
25. Brown JS, Banerji U. Maximising the potential of AKT inhibitors as anti-cancer treatments. *Pharmacol Ther*. 2017;172:101–115. doi:10.1016/j.pharmthera.2016.12.001
26. Yamaguchi T, Kakefuda R, Tajima N, Sowa Y, Sakai T. Antitumor activities of JTP-74057 (GSK1120212), a novel MEK1/2 inhibitor, on colorectal cancer cell lines *in vitro* and *in vivo*. *Int J Oncol*. 2011;39:23–31. doi:10.3892/ijo.2011.1015
27. Yoshida T, Kakegawa J, Yamaguchi T, et al. Identification and Characterization of a Novel Chemotype MEK Inhibitor Able to Alter the Phosphorylation State of MEK1/2. *Oncotarget*. 2012;3:1533–1545. doi:10.18632/oncotarget.747
28. Khan ZM, Real AM, Marsiglia WM, et al. Structural basis for the action of the drug trametinib at KSR-bound MEK. *Nature*. 2020;588:509–514. doi:10.1038/s41586-020-2760-4
29. Yan L. Abstract #DDT01-1: MK-2206: A potent oral allosteric AKT inhibitor. *Cancer Res*. 2009;69(9_Supplement):DDT01-1-DDT01-1.
30. Kunishima M, Kawachi C, Iwasaki F, Terao K, Tani S. Synthesis and characterization of 4-(4,6-dimethoxy-1,3,5-triazin-2-yl)-4-methylmorpholinium chloride. *Tetrahedron Lett*. 1999;40:5327–5330. doi:10.1016/S0040-4039(99)00968-5
31. Kunishima M, Kawachi C, Morita J, Terao K, Iwasaki F, Tani S. 4-(4,6-dimethoxy-1,3,5-triazin-2-yl)-4-methyl-morpholinium chloride: an efficient condensing agent leading to the formation of amides and esters. *Tetrahedron*. 1999;55:13159–13170. doi:10.1016/S0040-4020(99)00809-1
32. Wang G, Zhao L, Jiang Q, et al. Intestinal OCTN2- and MCT1-targeted drug delivery to improve oral bioavailability. *Asian J Pharm Sci*. 2020;15:158–172. doi:10.1016/j.ajps.2020.02.002
33. Cametti M, Crousse B, Metrangolo P, Milani R, Resnati G. The fluorous effect in biomolecular applications. *Chem Soc Rev*. 2012;41:31–42. doi:10.1039/c1cs15084g
34. Arakawa H, Kubo H, Washio I, et al. Rat Kidney Slices for Evaluation of Apical Membrane Transporters in Proximal Tubular Cells. *J Pharm Sci*. 2019;108:2798–2804. doi:10.1016/j.xphs.2019.03.031
35. Caldwell JJ, Davies TG, Donald A, et al. Identification of 4-(4-Aminopiperidin-1-yl)-7*H*-pyrrolo[2,3-*d*]pyrimidines as Selective Inhibitors of Protein Kinase B through Fragment Elaboration. *J Med Chem*. 2008;51:2147–2157. doi:10.1021/jm701437d
36. Freeman-Cook KD, Autry C, Borzillo G, et al. Design of Selective, ATP-Competitive Inhibitors of Akt. *J Med Chem*. 2010;53:4615–4622. doi:10.1021/jm1003842
37. Uesaka M, Saito Y, Yoshioka S, Domoto Y, Fujita M, Inokuma Y. Oligoacetylacetones as shapable carbon chains and their transformation to oligoimines for construction of metal-organic architectures. *Commun Chem*. 2018;1:1–7. doi:10.1038/s42004-018-0021-3
38. Kunishima M, Yamamoto K, Watanabe Y, Hioki K, Tani S. Development of novel polymer-type

dehydrocondensing reagents comprised of chlorotriazines. *Chem Commun*. 2005:2698–2700. doi:10.1039/b501917f

39. Sato D, Wu Z, Fujita H, Lindsey JS. Design, Synthesis, and Utility of Defined Molecular Scaffolds. *Organics*. 2021;2:161–273. doi:10.3390/org2030013

40. Green LM, Reade JL, Ware CF. Rapid colormetric assay for cell viability: Application to the quantitation of cytotoxic and growth inhibitory lymphokines. *J Immunol Methods*. 1984;70:257–268. doi:10.1016/0022-1759(84)90190-X

41. Yamaoka K, Nakagawa T, Uno T. Statistical Moments in Pharmacokinetics. *J Pharmacokinet Biopharm*. 1978;6:547–558. doi:10.1007/BF01062109